Journal Pre-proof
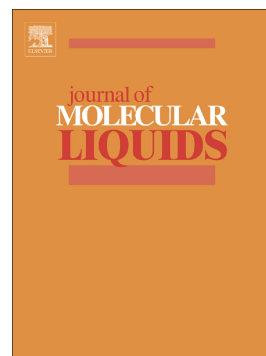
Densification and tribofilm formation in hydrocarbon nanofluids induced by MoS2 nanotubes

Loukia Maritsa, Alfredo Bol, Santiago Aparicio

Please cite this article as: L. Maritsa, A. Bol and S. Aparicio, Densification and tribofilm formation in hydrocarbon nanofluids induced by MoS2 nanotubes, *Journal of Molecular Liquids* (2020), https://doi.org/10.1016/j.molliq.2020.113291

This is a PDF file of an article that has undergone enhancements after acceptance, such as the addition of a cover page and metadata, and formatting for readability, but it is not yet the definitive version of record. This version will undergo additional copyediting, typesetting and review before it is published in its final form, but we are providing this version to give early visibility of the article. Please note that, during the production process, errors may be discovered which could affect the content, and all legal disclaimers that apply to the journal pertain.

Densification and tribofilm formation in hydrocarbon nanofluids induced by MoS_2 nanotubes

Loukia Maritsa,[a] Alfredo Bol[*a,b] and Santiago Aparicio[*a,c]

[a] International Research Center in Critical Raw Materials for Advanced Industrial Technologies (ICCRAM). University of Burgos, 09001 Burgos, Spain

[b] Department of Physics, University of Burgos, 09001 Burgos, Spain

[c] Department of Chemistry, University of Burgos, 09001 Burgos, Spain

*Corresponding Authors: alf_bol@ubu.es (A. Bol) and sapar@ubu.es (S. Aparicio)

ABSTRACT: The nanoscopic behaviour of dispersions of MoS_2 nanotubes in hydrocarbons were studied by molecular dynamics simulations. The reported results allowed the analysis of hydrocarbons adsorption at nanotubes external wall as well as the behaviour of the confined phase of hydrocarbons inside the nanotubes internal cavity. The adsorption and confinement of hydrocarbons leads to large structural rearrangements in the vicinity of the nanotubes in comparison with bulk liquid phase, which are pivotal for the behaviour of these nanofluids as lubricant media. The large affinity of the considered hydrocarbons for the nanotubes surfaces and cavities determines the stability of the considered dispersions and it allows the application of these nanofluids for several technologies in particular for enhanced lubrication.

Keywords: MoS_2 nanotubes; hydrocarbons; molecular dynamics; nanofluids; solvation; confinement.

nanotubes in oil dispersions

adsorption → ← confinement

molecular dynamics nanoscopic features
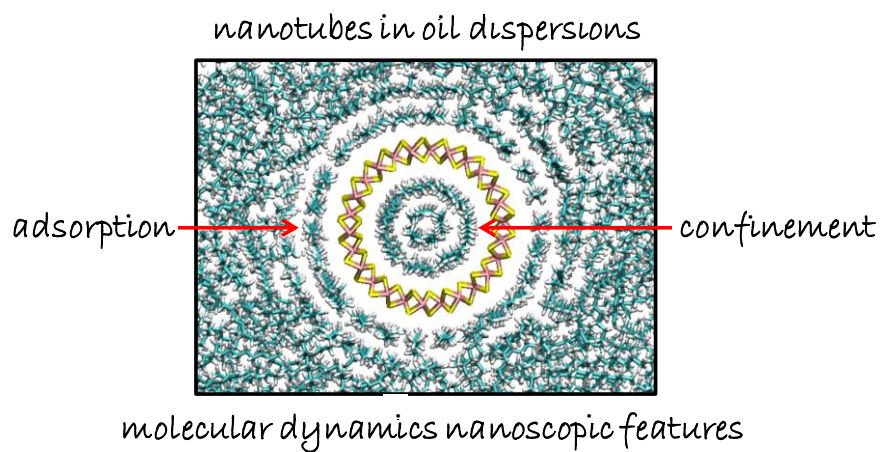
Graphical abstract

1. Introduction

The modification of lubricant oils properties by the addition of nanoparticles has been widely considered in the literature [1,2]. A large collection of different nanomaterials has been considered [3], and thus different mechanisms of lubrication [4], but the global objective for nanoparticles dispersion in base oils is to reduce friction and wear, thus improving oils tribological performance [5]. Among the studied materials, Transition Metal Dichalcogenides (TMDs) nanoparticles have been considered as oil additives because of their excellent frictional performance [6]. Thus, TMDs – nanoparticles [7,8], considering compounds such as MoS_2 [9] or WS_2 [10] have been largely tested under several tribological conditions and environments. TMDs nanoparticles as base oils additives have been considered in different forms, including fullerene-like [11], 2D monolayers [12,13] as well as nanotubes [14] and quantum dots [15].

The case of TMDs nanotubes has been widely studied in the literature showing excellent performance as base oil additives. Kalin et al. [16] considered MoS_2 multiwalled nanotubes (MWNTs) and showed a 2-times reduction of friction and 5-9 times lower wear, showing a remarkable improvement with regard to the base oil based on the formation of MWNTs tribofilm on the surfaces. The superior performance of MoS_2 nanotubes and the formation of tribofilms have been considered for different material such as Zinc – coated surfaces [14], steel [17] or steel coated with materials such as TiN, TiAlN and CrN [18]. Likewise, experimental studies on the combined use of MoS_2 nanotubes and conventional oil additives have proved a synergistic effect maintaining the superior performance of nanotubes [19] although antagonistic effects have also been reported for certain conditions [20].

The suitable performance of TMDs nanotubes as additives for industrial lubrication operations requires a knowledge of the behaviour of base oils plus TMDs nanotubes dispersion at the nanoscopic level. This nanoscopic point of view can be reached through computational chemistry tools such as molecular dynamics (MD) simulations, which may provide quantitative information on the behaviour of these systems. Although MD studies on the behaviour of TMDs nanotubes have been reported in the literature [21,22], the behaviour of TMDs + base oil dispersions has not been considered. Therefore, for the understanding the TMDs nanotubes role as lubricant additives the properties and structuring

of the corresponding dispersions in base oils have to be considered. The interaction of base oils with TMDs nanotubes is, in principle, twofold: with the outer and with the inner nanotube shells, whenever hydrocarbon molecules penetrate inside this cavity. As a consequence thereof, two effects are expected, oil adsorption on the outer shell and confinement in the inner cavity, and they should govern the properties of the formed dispersions. Therefore, to infer a nanoscopic characterization of base oil + TMDs nanotubes dispersions, a MD study is reported in this work. The base oil is modelled considering n-octane (C8) liquid phase and single walled MoS_2 nanotubes (MOSnt). Additional simulations were carried out considering longer hydrocarbons (octadecane, C18, and hexatriacontane, C36) in the liquid phase. The behaviour of the systems was studied as a function of temperature and the results were analysed in terms of the dispersion properties at the nanoscopic level with deeper insights into solvation and confinement mechanisms.

2. Methods

MD simulations were carried out with MDynaMix v.5.2 package [23]. The systems considered along this work were modelled using a MOSnt with length, L = 30 Å, external diameter, d_e = 25.9 Å, and internal diameter, d_i = 19.5 Å, Figure 1a. The MOSnt was placed with its long axis along the x axis and surrounded by hydrocarbon molecules (C8, C18, or C36), Figure 1b. The number of hydrocarbon molecules surrounding the MOSnt was selected to have roughly a constant number of carbon atoms (~ 10200) for all the considered hydrocarbons, thus allowing to analyse the effect of the hydrocarbon size on the nanofluid properties for a fixed content of carbons. The simulation box size was fixed considering the literature experimental density for neat hydrocarbons. The considered simulation boxes have 6.9 vol % (volume percentage) of MOSnt, calculated as suggested by Razmara et al. for carbon nanotubes [24], which mimics a highly concentrated nanofluid. Nevertheless, the MOSnt to MOSnt distance considering neighbour periodic cells is 4.2 and 4.6 nm for axial and longitudinal separations, which points to almost negligible MOSnt – MOSnt interactions, thus the behaviour of the studied systems is governed by alkane – MOSnt and alkane – alkane interactions. Initial simulation boxes were built with Packmol software [25].

The MOSnt was described using a forcefield parameterization developed by Sresht et al. [26] for MoS_2 monolayers, which was suitable for describing MoS_2 – liquid phase

interactions. The MOSnt was maintained fixed along the simulations, thus hydrocarbon – MOSnt interactions are governed by Lennard-Jones and coulombic terms of the forcefield, thus using Sresht et al. parameters [26] are a suitable option considering that these parameters should be the same both for monolayers and nanotubes. In the case of hydrocarbons, they were described using OPLS-AA force field [27].

Periodic boundary conditions in the three space directions were applied for all the MD simulations. NPT simulations at 1 bar and several temperatures were carried out. To analyse the temperature effect on nanofluids properties the MOSnt + C8 system was studied at 293, 313, 333, 353, 373 and 393 K, with the highest temperature being slightly below the C8 normal boiling point (398.7 K [28]). The effect of hydrocarbon length was studied considering MOSnt + C18 or + C36 systems at 353 K, above the melting temperature of both hydrocarbons [28]. Simulation production runs were carried out for 100 ns. The pressure and temperature of the systems were controlled by using Nose–Hoover method. The equations of motion were treated with the Tuckerman–Berne double time step algorithm [29]. Electrostatic interactions were handled with Ewald method (15 Å for cut-off radius) [30]. Lorentz-Berthelot mixing rules were applied for cross-term Lennard-Jones interactions (15 Å cut-off). The analysis and determination of properties from MD trajectories in the considered ensemble was carried out using VMD [31] and TRAVIS [32].

3. Results and discussion

The MD simulations carried out in this work elucidated the structuring of the considered hydrocarbons in MOSnt + alkane nanofluids. The structural changes in the properties of the liquid hydrocarbons because of the presence of MOSnt and the molecular arrangements of these alkanes around and inside the MOSnt should be produced by the affinity of these molecules for the MOSnt structure. This effect can be quantified by the interaction energy, E_{inter}, between the nanotube and the hydrocarbon molecules, Figure 2a. The reported results in Figure 2a show very large E_{inter} for all the considered alkanes. Likewise, the time evolution of E_{inter} shows that in roughly 0.1 ns the structures of alkanes around the MOSnt are equilibrated, thus confirming the affinity for the MOSnt surface and internal cavity. The comparison of E_{inter} for the considered hydrocarbons show the ordering (in absolute value) C18 > C8 > C36. For alkane – MOSnt interactions, the van der Waals interaction should have a prevailing role, and thus, larger hydrocarbons should have larger

E_{inter} because of the increase in van der Waals contacts. Nevertheless, results in Figure 2a show that this is only effective up to a certain number of carbon atoms, as inferred from the increase on going from C8 to C18, whereas when the alkane molecule is too long, as in the case of C36, E_{inter}, decreases remarkably (e.g. a 40 % decrease on going from C18 to C36), which can be justified considering the steric hindrance which decreases effective interaction with MOSnt external surface as well as hydrocarbon effective confinement inside the nanotube cavity. Nevertheless, the alkane – MOSnt interactions are very effective, in the case of C8 results in Figure 2a, an increase in temperature from 293 to 393 K leads to a decrease of only 8.5 % in E_{inter}, which is remarkable considering that at 393 K the alkane is only 5.7 K below its boiling temperature. Therefore, the alkane – MOSnt interactions are strong enough to be maintained in a wide temperature range thus maintaining nanofluids properties in a wide operational range.

The presence of MOSnt and the corresponding changes in alkane liquid structuring can be quantified through E_{inter} for alkane – alkane interactions, Figure 2b. These results confirm that MOSnt reinforces alkane – alkane interactions for all the considered alkanes and in a wide temperature range. Therefore, MOSnt – alkane nanofluids are characterized by very effective alkane interactions with the nanotube as well as a subsequent strengthening of interactions between the hydrocarbons. As the alkane – alkane interactions have a van der Waals nature, the presence of MOSnt induces an increase of these forces by the increase of carbon to carbon contacts, thus, it can be inferred that alkanes could be more ordered in MOSnt-alkane nanofluids than in neat liquid hydrocarbon phases [33].

The interaction between the hydrocarbons and the MOSnt should lead to the penetration of alkane molecules in the internal cavity of the nanotube, thus forming a confined hydrocarbon phase. Results in Figure 3 shows the number of hydrocarbon molecules inside the MOSnt cavity starting from an empty cavity as a function of simulation time. The reported results show how alkane molecules penetrate into the MOSnt cavity reaching a steady composition at roughly 0.4 ns, for all the considered hydrocarbons and temperatures. For C8, a slight decrease in the number of confined atoms is inferred with increasing temperature, although a minor 3.6 % decrease is inferred in a 100 K range. Likewise, the increase in the hydrocarbon length increases the number of confined carbon atoms, although this increase is very minor, thus confirming that all the hydrocarbons are able to penetrate effectively inside the cavity and remains into the cavity even upon heating.

An additional simulation was carried out to analyse the alkane – MOSnt potential energy landscape considering a single C8 molecule placed outside the MOSnt at a distance d of the nanotube entry, with the centre of mass of C8 in the nanotube long axis, which is shifted along the nanotube long axis, Figure 4. The E_{inter} for MOSnt – C8 along the shifting is reported in Figure 4. The reported results show an stabilization of C8 molecule upon approaching to the nanotube opening, when the C8 molecule penetrates into the nanocavity an oscillatory behaviour is inferred corresponding to the placing of the Hs and Cs atoms with regard to the MOSnt periodic structure. A symmetrical behaviour is inferred when the C8 molecules leaves the MOSnt cavity. These results show a strong affinity of C8 for the internal cavity, even when a single molecule is considered and the molecule is placed in the centre of the cavity, which supports the fast and efficient penetration of C8 molecules in the nanotube cavity. In an additional simulation a single C36 molecule was placed outside the MOSnt and MD simulations were carried out without any restriction, the reported results in Figure 5, show how even this large molecule, which length is larger than the MOSnt length, is able to penetrate into the nanocavity being adsorbed into the internal wall, thus allowing all its C atoms to be interacting with the nanotube internal surface following an helicoidal pattern upon confined to improve van der Waals interactions. These results confirm that even very long hydrocarbons can be confined rearranging their shape to interact with the nanotube atoms.

A detailed analysis of the alkane structuring around and inside the MOSnt is reported in Figure 6. Result for C8 show large rearrangement of the liquid alkane in response to the MOSnt presence both outside and inside the nanotube in the 293 to 393 K range. Regarding the external solvation shell, C8 molecules develop up to three well defined separated adsorbed layers, which are maintained in the studied temperature range. The reported snapshots, and the corresponding average distributions in Figure 6, confirm highly ordered fluids outside the MOSnt. The external adsorbed layers, specially the first one in close contact with the MOSnt surface, show spots corresponding to C8 molecules aligned with the nanotube long axis. Additionally, the C8 arrangement in successive adsorbed layers follows a rhombic pattern, with molecules in the top layer shifted regarding the lower one, thus maintaining C8-C8 interactions as well as effective C8 – surface van der Waals contacts. In the case of confined C8 molecules, two shells are inferred, one following and in close contact with the nanotube surface and another one around the nanotube long axis. Likewise, results

7

in Figure 6 show that external adsorbed layers and internal, confined layers, are connected by a group of C8 molecules placed perpendicular to the nanotube long axis close to the nanotube opening. This highly ordered structuring in the vicinity of MOSnt is confirmed in Figure 7, in which the C8 caps in the vicinity of the nanotube openings as well as the C8 molecules aligned with the nanotube axis are confirmed (green arrows). The position of the adsorbed and confined layers is quantified by number density profiles in the perpendicular direction to the MOSnt long axis, Figure 8. For the external C8 region up to four peaks are inferred, with the larger densification for the first peak in the vicinity of the MOSnt external surface. This first peak is placed at 3.5 Å of the S atoms in the MOSnt surface and the additional outer peaks are separated 4.3 Å. In the case of confined C8, the first layer is placed at 4.3 Å of the internal surface, which is larger than the distance for the external adsorbed layer. This can be justified considering the curvature and its effect on the alkane packing when confined. The second confined layer is placed around the centre of the nanotube. Therefore, the reported results show the formation of adsorbed and confined layers, which lead to very efficient MOSnt – C8 interactions. These interactions are very efficient in the whole temperature range, Figure 6, and only a very minor weakening is inferred upon heating, as confirmed by the temperature evolution of E_{inter} reported in Figure 9. The weakening of E_{inter} upon heating is related with the increase in molecular mobility but maintaining most of the features of confined and adsorbed molecules, Figure 6.

The alkane molecules in adsorbed and confined regions are highly ordered, and this effect leads to reinforcement of alkane-alkane interactions, Figure 2b, which should be justified considering changes in the way alkane molecules interact between each other. This effect was quantified through the use of centre-of-mass Radial Distribution Functions, RDFs, for alkane-alkane pairs as reported in Figure 10 for C8 as a function of temperature. RDFs for confined, Figure 10a, and adsorbed, Figure 10b, regions are totally different to those in pseudobulk, i.e. non-perturbed liquid C8, Figure 10c regions. A striking densification effect is detected by the value of RDFs: its maxima are, with respect to the values of bulk liquid C8, 15 times higher and 5 times higher for confined and adsorbed regions, respectively. But not only confined and adsorbed RDFs peak values differ, also position: the first RDF peak, corresponding to C8 molecules in the nearest region around a central C8 molecule, is placed at 5.2 Å whereas for C8 molecules in confined and adsorbed regions this peak appears at roughly 1 Å closer, i.e. C8 molecules are in closer contact upon adsorption or confinement in

MOSnt in comparison with bulk liquid C8, thus C8-C8 interactions are stronger, Figure 2b. This effect for the first solvation shell is also reproduced for external shells, further peaks in Figure 10, especially for confined C8. Hence a general contraction of the hydrocarbon molecules pattern is produced by the presence of the MOSnt. Solvation numbers calculated from RDFs, Figure 11, confirm this explanation: they are larger for bulk liquid phase in comparison with confined and adsorbed layers because of the highly directional arrangement of alkane molecules as reported in Figure 7 in comparison with a random much less ordered structure in absence of the nanotube. This allows a larger number of C8 molecules around a central one. Nevertheless, solvation numbers in Figure 11 for confined and adsorbed fluids are large enough considering the limited size of these regions and the directionality of the interactions.

The strength of the developed interactions, Figure 2, as well as the highly ordered structuring in response to MOSnt presence, Figures 6 and 7, should lead to changes in the dynamic properties of the hydrocarbons in MOSnt + alkane nanofluids. This behaviour was quantified through self-diffusion coefficients, D, as calculated from mean square displacements and Einstein's equation for molecules in different regions around the MOSnt and compared with experimental D data from the literature [34], Table 1. The confined and adsorbed molecules in the first layer have very low D values, which agrees with strong C8-MOSnt and C8-C8 interactions, whereas molecules in the second external adsorbed layer show an order of magnitude larger than those in the first adsorbed layer, thus confirming the prevailing role of C8 − MOSnt interactions for the determination of these properties. Values in the pseudobulk region are in excellent agreement with experimental data from the literature, showing the suitability of the used MD approach for predicting the properties of these nanofluids. Therefore, dynamic properties of confined and directly adsorbed alkane molecules are completely different to those in bulk liquid hydrocarbon, thus confirming the role of MOSnt as a disrupting agent on the hydrocarbon's physical properties as well as the large affinity for the MOSnt.

The effect of the alkane chain length on ordering inside and outside MOSnt is further analysed in Figure 12 for C18 (analogous results are inferred for C36). Results in Figure 12a shows the development of confined and adsorbed layers similar to those for shorter hydrocarbons (C8 in Figures 6 and 7). Nevertheless, profiles in Figure 12a show more defined spots both for confined and adsorbed C18 molecules, which point to molecules developing

better alignment with the nanotube for certain regions. Results in Figure 12b show that most of the nanotube first external adsorbed layer is characterized by C18 molecules perfectly aligned with the nanotube long axis whereas in other regions molecules are perpendicular, red arrows in Figure 12. Likewise, C18 molecules inside the MOSnt cavity, Figure 12c, adopt a perfect alignment with the axis for those molecules in the vicinity of the nanocavity centre, whereas those close to the internal surface adopt a spiral-like orientation to allow the fitting of the larger C18 molecules in comparison with shorter C8 alkane. Therefore, the increase in alkane chain length also leads to confinement and adsorption of hydrocarbon molecules but the size of the molecules leads to changes in the molecular arrangements in comparison with shorter compounds to allow efficient alkane – MOSnt interactions. Likewise, results in Figure 13 show that for large alkanes, C18, the presence of MOSnt induces changes in alkane self-aggregation well – beyond those regions in the vicinity of the nanotube, thus leading to clusters of hydrocarbons with parallel arrangements improving alkane – alkane van der Waals interactions. Therefore, the structuring and properties of liquid alkanes is even more disrupted when the alkane chain length increases leading to efficient interactions with the MOSnt as well as strengthening alkane-alkane intermolecular forces and leading to alkane clustering.

4. Conclusions

The properties of hydrocarbon – MoS_2 nanotube systems are analysed considering molecular dynamics simulations as a function of temperature and alkane chain length. The reported results show strong affinity of the considered hydrocarbons for the nanotube, which lead to highly ordered adsorbed and confined alkane layers. The structure of liquid hydrocarbon is rearranged in the external solvation shell of the nanotube leading to ordered layers following the nanotube symmetry and extending well beyond those molecules in close contact with the surface which precludes building of an efficient extended tribolayer in dynamic conditions. This liquid hydrocarbon restructuring around the nanotube and the strong interaction between both systems can be considered as the building up of an effective antiwear coating, explaining antiwear MoS_2 properties [14,15,16]. In the case of confined molecules, they develop also patterns in the region around the nanotube centre as well as in the vicinity of the internal nanotube surface. These structural changes lead to large

interaction energies which decrease molecular mobility of the hydrocarbon molecules in the neighbourhood of the nanotube. The perturbative effects of the nanotube are larger when the hydrocarbon chain increases. The provided nanoscopic characterizations probes that alkane properties can be dramatically changed and fine-tuned by the addition of controlled amounts of MoS_2 nanotubes, which is relevant for technological applications such as lubrication.

Acknowledgement

References

[1] W. Dai, B. Kheireddin, H. Gao, H. Liang, Roles of nanoparticles in oil lubrication. Tribol. Int. 102 (2016) 88-98.

[2] Y. Chen, P. Ranner, H. Liang, Dispersion of nanoparticles in lubricating oil: a critical review. Lubricants 7 (2019) 7.

[3] S. Shahnazar, S. Bagheri, S.B. Abd-Hamid, Enhancing lubricant properties by nanoparticle additives. Int. J. Hydrogen Energ. 41 (2016) 3153-3170.

[4] M. Gulzar, H.H. Masjuki, M.A. Kalam, M.Varman, N.W.M. Zulkifli, R.A. Mufti, R. Zahid, Tribological performance of nanoparticles as lubricating oil additives. J. Nanopart. Res. 18 (2016) 223.

[5] M.S. Charoo, M. Hanief, Improving the tribological characteristics of a lubricating oil by nano sized additives. Mater. Today Proc. (2020) DOI: j.matpr.2020.01.219

[6] M. Rodríguez-Ripol, A,M. Tomala, L.Pirker, M. Remskar, In-Situ formation of MoS_2 and WS_2 tribofilms by the synergy between transition metal oxide nanoparticles and sulphur-containing oil additives. Tribol. Lett. 68 (2020) 41.

[7] N.G. Demas, E.V. Timofeeva, J.L. Routbort, G.R. Fenske, Tribological effects of BN and MoS_2 nanoparticles added to polyalphaolefin oil in piston skirt/cylinder liner tests. Tribol Lett 47 (2012) 91–102.

[8] H. Sade, A. Moshkovich, J.P. Lellouche, L. Rapoport, Testing of WS_2 nanoparticles functionalized by a humin-like shell as lubricant additives. Lubricants 6 (2018) 3.

[9] Y. Jazaa, T. Lan, S. Padalkar, S. Sundarajan, The effect of agglomeration reduction on the tribological behavior of WS_2 and MoS_2 nanoparticle additives in the boundary lubrication regime. Lubricants 6 (2018) 106.

[10] M. Raoi, V.B. Niste, J. Walker, J. Zekonyte, Mechanism of Action of WS_2 Lubricant Nanoadditives in High-Pressure Contacts. Tribol. Lett. 52 (2013) 81-91.

[11] J. Kogovšek, M. Kalin, Various MoS_2-, WS_2- and C-based micro- and nanoparticles in boundary lubrication. Tribol. Lett. 2014, 53, 585–597.

[12] N. Rajendhram, S. Palanisamy, P. Periyasamy, R. Venkatachalam, Enhancing of the tribological characteristics of the lubricant oils using Ni-promoted MoS_2 nanosheets as nano-additives. Tribol. Int. 118 (2018) 314-328.

[13] Y. Liu, Y. Liu, T. Ma, J. Luo, Atomic Scale Simulation on the anti-pressure and friction reduction mechanisms of MoS_2 monolayer. Materials 11 (2018) 683.

[14] M. Rodriguez-Ripoll, A.M. Tomala, V. Tontolin, M. Remskar, Performance of nanolubricants containing MoS_2 nanotubes during form tapping of zinc-coated automotive components. J. Manuf. Process. 39 (2019) 167-180.

[15] J. Guo, R. Peng, H. Du, Y. Shen, Y. Li, J. Li, G. Dong, The application of nano-MoS_2 quantum dots as liquid lubricant additive for tribological behavior improvement. Nanomaterials 10 (2020) 200.

[16] M. Kalin, J. Kogovsek, M. remskar, Mechanisms and improvements in the friction and wear behavior using MoS_2 nanotubes as potential oil additives. Wear 280-281 (2012) 36-45.

[17] J. Kogovsek, M. Remskar, A.Mrzel, M. Kalin, Influence of surface roughness and running-in on the lubrication of steel surfaces with oil containing MoS_2 nanotubes in all lubrication regimes. Tribol. Int. 61 (2013) 40-47.

[18] S. Paskvale, M. Remskar, M. Cekada, Tribological performance of TiN, TiAlN and CrN hard coatings lubricated by MoS_2 nanotubes in Polyalphaolefin oil. Wear 352-353 (2016) 72-78.

[19] A. Tomala, M. Rodríguez-Ripoll, C. Gabler, M. Remskar, M. Kalin, Interactions between MoS_2 nanotubes and conventional additives in model oils. Tribol. Int. 110 (2017) 140-150.

[20] A. Tomala, M. Rodríguez-Ripoll, J. Kogovsek, M. Kalin, A. Bednarska, R. Michalczewski, M. Szcerek, Synergisms and antagonisms between MoS_2 nanotubes and representative oil additives under various contact conditions. Tribol. Int. 129 (2019) 137-150.

[21] M. Stefanov, A.N. Enyashin, T. Heine, G. Seifert, Nanolubrication: how Do MoS_2-based nanostructures lubricate? J. Phys. Chem. C 112 (2008) 17764-17767.

[22] M. Dallavalle, N. Sandig, F. Zerbetto, Stability, dynamics, and lubrication of MoS_2 platelets and nanotubes, Langmuir 28 (2012) 7393-7400.

[23] A.P. Lyubartsev, A.M. Laaksonen, MDynaMix - a scalable portable parallel MD simulation package for arbitrary molecular mixtures. Comput. Phys. Commun. 2000, 128, 565–589.

[24] J. Koca, Z. Jirouskova, R. Svobodova Varekova, J. Vanek, Electronegativity equalization method: parameterization and validation for organic molecules using the merz-kollman-singh charge distribution scheme. J. Comput. Chem. 2009, 30, 1174–1178.

[25] V. Sresht, A.G. Rajan, E. Bordes, M.S. Starno, A.A.H. Pádia, D. Blankschtein, Quantitative modeling of MoS2–solvent interfaces: predicting contact angles and exfoliation performance using molecular dynamics. J. Phys. Chem. C 2017, 121, 9022-9031.

[26] S.W.I. Siu, K. Pñukackova, R.A. Böckman, Optimization of the OPLS-AA force field for long hydrocarbons. J. Chem. Theory Comput. 8 (2012) 1459-1470.

[27] W. E. Acree, J. S. Chickos, NIST Chemistry WebBook, NIST Standard Reference Database Number 69, Eds. P.J. Linstrom and W.G. Mallard, National Institute of Standards and Technology, Gaithersburg MD, 20899, https://doi.org/10.18434/T4D303, (accesed April 6, 2020).

[28] M. Tuckerman, B. J. Berne, G. J. Martyna, Reversible multiple time scale molecular dynamics. J. Chem. Phys. 97 (1992) 1990-2001.

[29] U. L. Essmann, M. L. Perera, T. Berkowitz, H. Darden, H. Lee, L. G. Pedersen, A smooth particle mesh Ewald method. J. Chem. Phys. 103 (1995) 8577-8593.

[30] W. Humphrey, A. Dalke, K. Schulten, VMD - visual molecular dynamics, J. Molec. Graphics 14 (1996) 33-38.

[31] M. Brehm, B. Kirchner, TRAVIS - A free Analyzer and Visualizer for Monte Carlo and Molecular Dynamics Trajectories, J. Chem. Inf. Model. 51 (2011), 2007-2023.

[32] P.S. Tofts, D. Lloyd, C.A. Clark, G.J. Barker, G.J.M. Parker, P. McConville, C.Baldock, J.M. Pope, Test Liquids for Quantitative MRI Measurements of Self-Diffusion Coefficient In Vivo, Magn. Reson. Med. 43 (2000) 368-374.

[33] A. Goursot, T. Mineva, R. Kevorkyants, D.Talbi, Interaction between n-alkane chains: applicability of the empirically corrected density functional theory for van der waals complexes. J. Chem. Theory Comput. 3 (2007) 755-763.

[34] P.S. Tofts, D. Lloyd, C.A. Clark, G.J. Barker, G.J.M. Parker, P. McConville, C.Baldock, J.M. Pope, Test Liquids for Quantitative MRI Measurements of Self-Diffusion Coefficient In Vivo, Magn. Reson. Med. 43 (2000) 368-374.

Table 1

Self-diffusion coefficient, D, for C8 molecules in different regions for MOSnt + C8 nanofluids at 293 K. Experimental data for liquid C8 from Tofts et al. [34].

region	$10^9 D$ / m^2 s^{-1}
confined	5.1 ± 0.6
1st layer	19.5 ± 2.1
2nd layer	132.1 ± 10.4
pseudobulk	197.8 ± 16.1
experimental	214

Table 1

Figure Captions

Figure 1. (a) MOSnt used in this work showing diameters and length, (b) MOSnt + hydrocarbon cubic box used for MD simulations. In panel b, blue lines show periodic boundary conditions. Front and side views are reported inside each panel.

Figure 2. Interaction energy, E_{inter} (sum of electrostatic and Lennard-Jones contributions), for MOSnt + alkane nanofluids, considering the type of alkane and temperature. Results in panel a show E_{inter} for MOSnt – alkane interactions; results in panel b show E_{inter} for alkane – alkane interactions. The values of E_{inter} are reported vs simulation time, t, starting (t = 0) from configurations reported in Figure 1b. Values inside each panel shows average after equilibration (last 10 ns of the simulations).

Figure 3. Number of carbon atoms, N_C, inside MOSnt internal cavity, for MOSnt + alkane nanofluids, as a function of simulation time, starting from empty cavities, and considering the type of alkane and temperature.

Figure 4. Interaction energy, E_{inter} (sum of electrostatic and Lennard-Jones contributions), for MOSnt + alkane nanofluids as a single C8 molecules penetrates inside the MOSnt internal cavity along its longitudinal axis (indicated by black arrow). Results are reported with reference to the opening of the MOSnt as a function of distance, d, of C8 centre of mass (red cross), indicated as red arrow. Dashed red lines indicate the position of the MOSnt. Value inside the panel indicated in red shows the average value of E_{inter} for d in the 0 to 30 Å range.

Figure 5. Evolution of a single C36 molecule placed along the MOSnt in the vicinity of MOSnt opening after 20 ps of simulation at 353 K.

Figure 6. Analysis of C8 distribution around and inside MOSnt as a function of temperature. Results in panels (a,d,g) show snapshots at the end of simulations (after 100 ns); results in panels (b,e,g) shows front and (c,h,i) lateral (along the MOSnt long axis) vision of average distribution of C8 molecules. Rhomboidal patterns for C8 arrangements are reported in panels (b,e,g). The MOSnt is indicated in panels (c,h,j) in yellow lines. Results for MOSnt + C8 nanofluids.

Figure 7. Distribution of C8 molecules around and inside MOSnt at 293 K showing (a) front and (b) side views. In panel a, rhomboidal patterns are showed in green. In panel b, shell on the entry of MOSnt and alignment of C8 molecules in the external shells are showed with green arrows. A scheme of the external solvation shell around MOSnt is reported at the bottom of panel b. Results for MOSnt + C8 nanofluids.

Figure 8. Number density profile, ρ, in the direction perpendicular to the long axis of MOSnt for MOSnt + C8 nanofluids at 293 K. r = 0 corresponds to MOSnt center. The dashed lines show the position of the internal and external MOSnt surface. Gray area shows the MOSnt. Red labels and arrows indicate the distances to the internal and external MOSnt surfaces for relevant C8 confined and adsorbed layers.

Figure 9. Temperature evolution of E_{inter} (sum of electrostatic and Lennard-Jones contributions), for MOSnt + C8 interactions in MOSnt + C8 nanofluids.

Figure 10. Center-of-mass radial distribution function, $g(r)$, for C8-C8 pairs in MOSnt + C8 nanofluids at 293 K. Results are reported for C8 molecules confined inside MOSnt cavity, C8 molecules in the first external solvation shell of MOSnt and in the pseudobulk region (C8 molecules 2 nm beyond the first adsorbed shell). Values inside the panels indicate the position of the first peak and dashed lines are reported for comparison purposes.

Figure 11. Solvation numbers, N, obtained from the integration of radial distribution functions in Figure 8 around a central C8 molecule in MOSnt + C8 nanofluids at 293 K for the considered regions. Values inside the panels indicate Ns for the first solvation shell around C8, defined with r = 7.5 Å.

Figure 12. Analysis of C18 distribution around and inside MOSnt as a function of temperature. Results in panel a show front vision of average distribution of C18 molecules. Results in panel b show distribution of C18 molecules in the first external adsorbed layer on MOSnt and in panel b for C18 molecules confined inside the MOSnt internal cavity. Red arrows in panel b indicate C18 molecules aligned with the MOSnt long axis and molecules perpendicular to this axis. Red arrows in panel c show C18 molecules in the first confined layer following an helicoidal pattern as well as C18 molecules along the long MOSnt axis. Results for MOSnt + C18 nanofluids.

Figure 13. Distribution of C18 molecules in the vicinity of MOSnt for C18 + MOSnt nanofluid at 293 K.
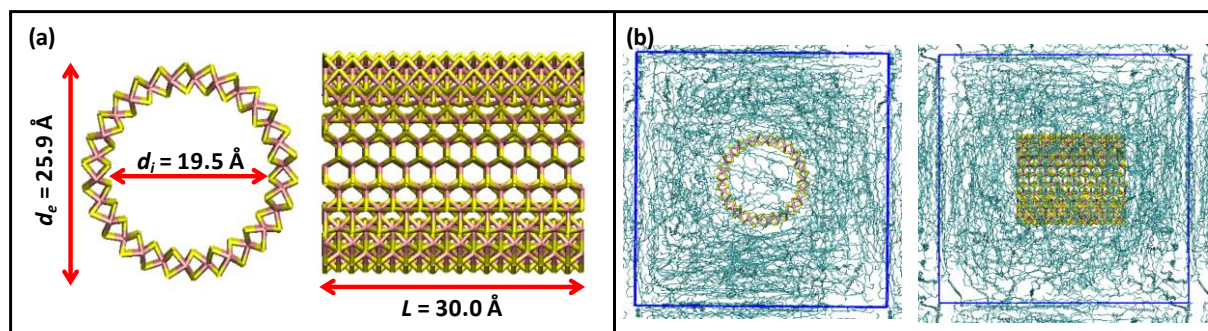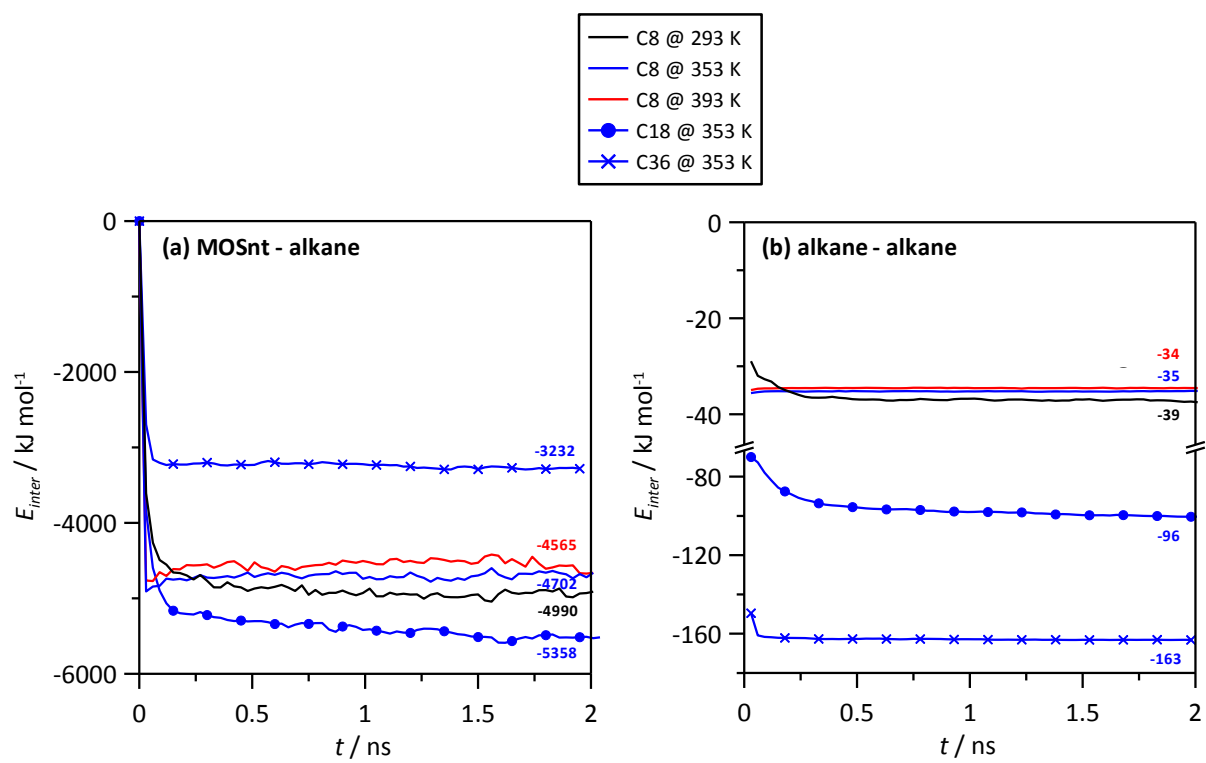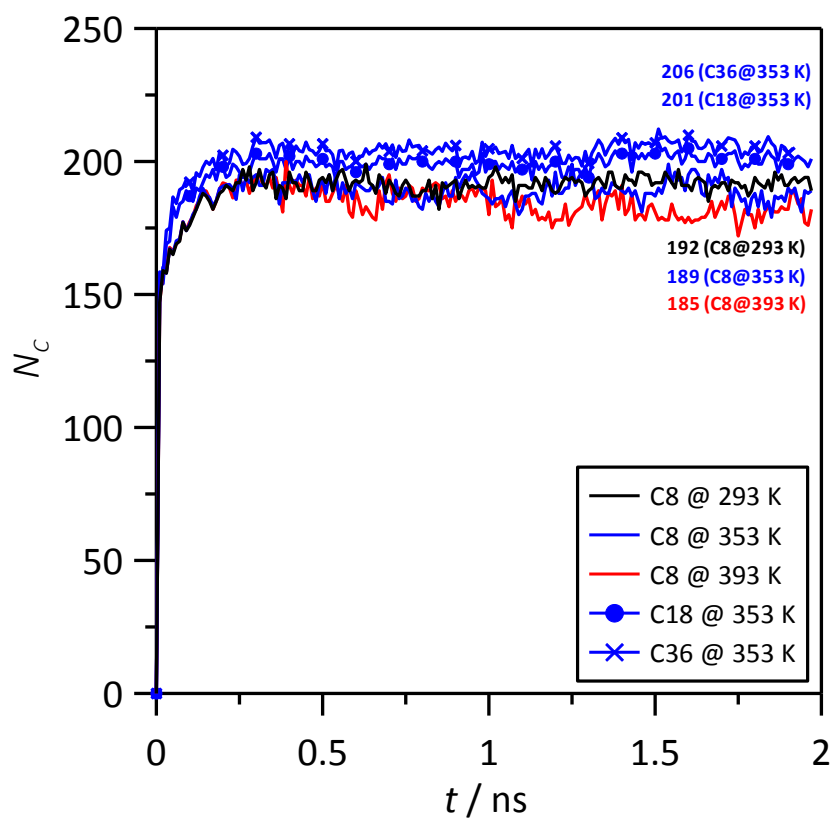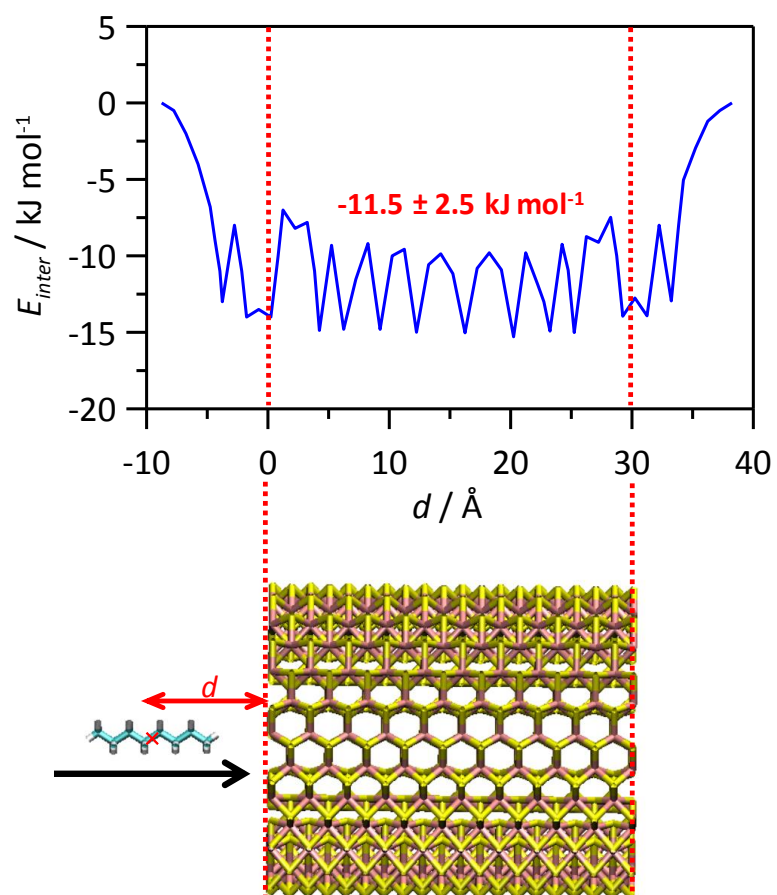
Figure 1

Figure 2

Figure 3

Figure 4

t = 20 ps

Figure 5

293 K   353 K   393 K
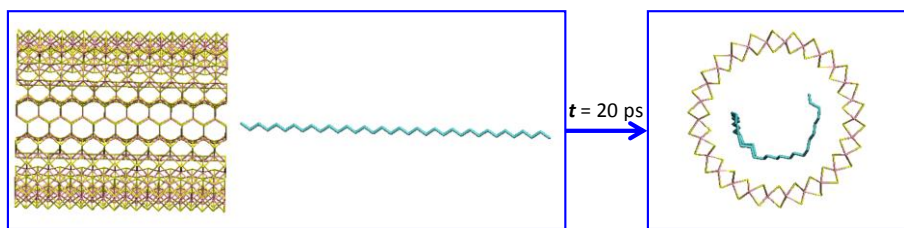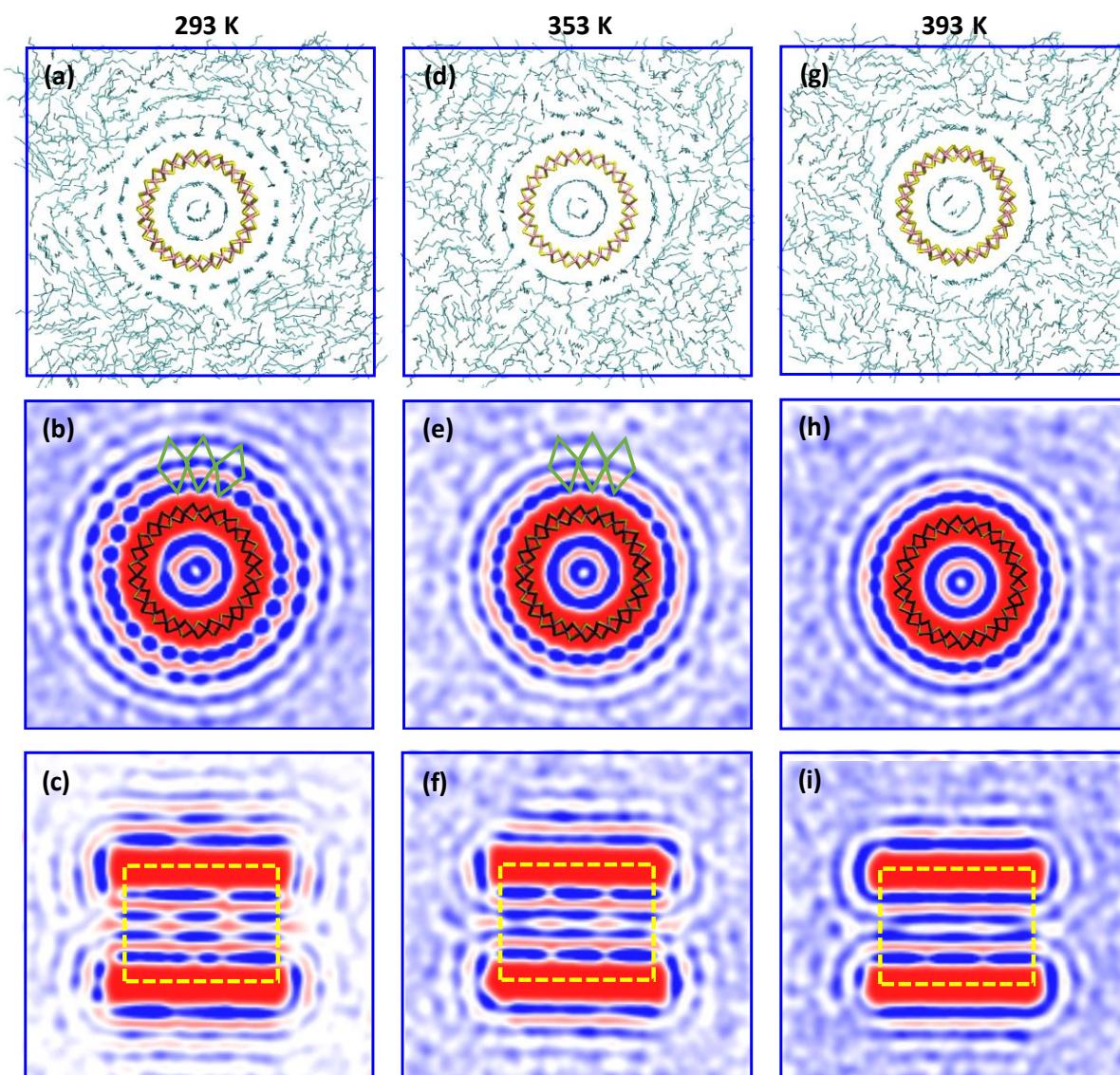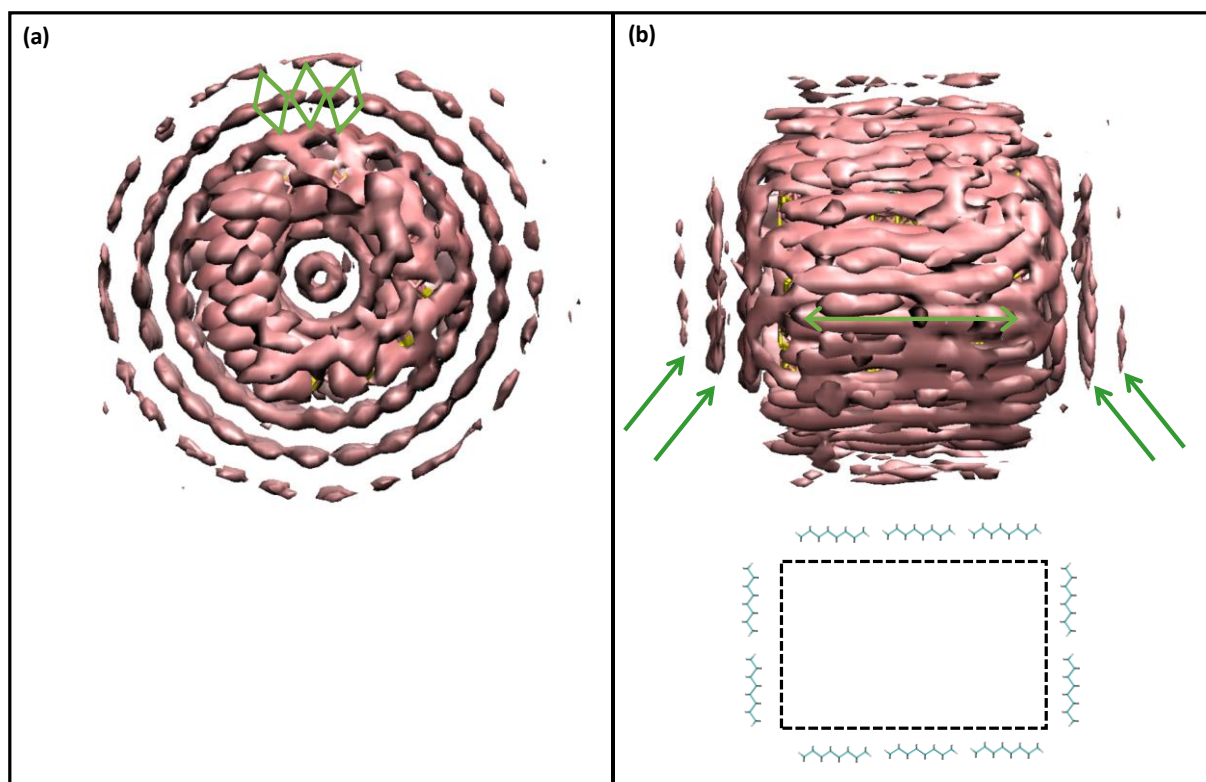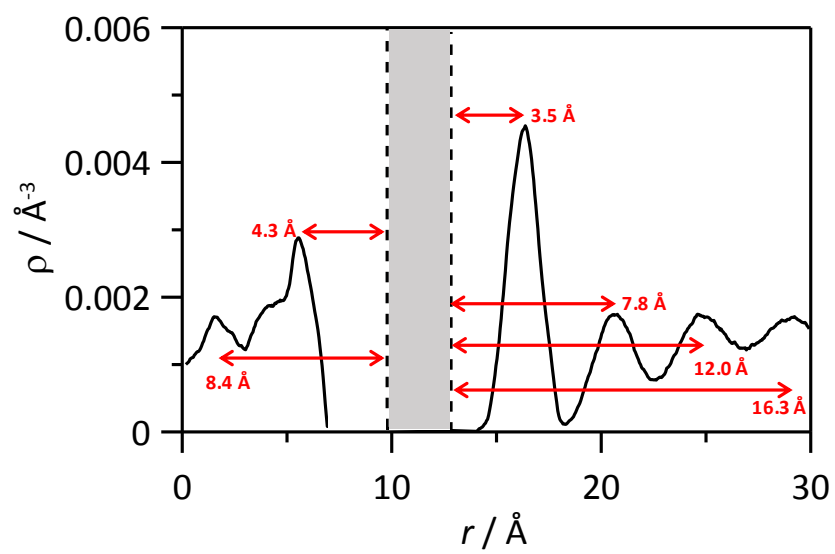
Figure 6

Figure 7

Figure 8
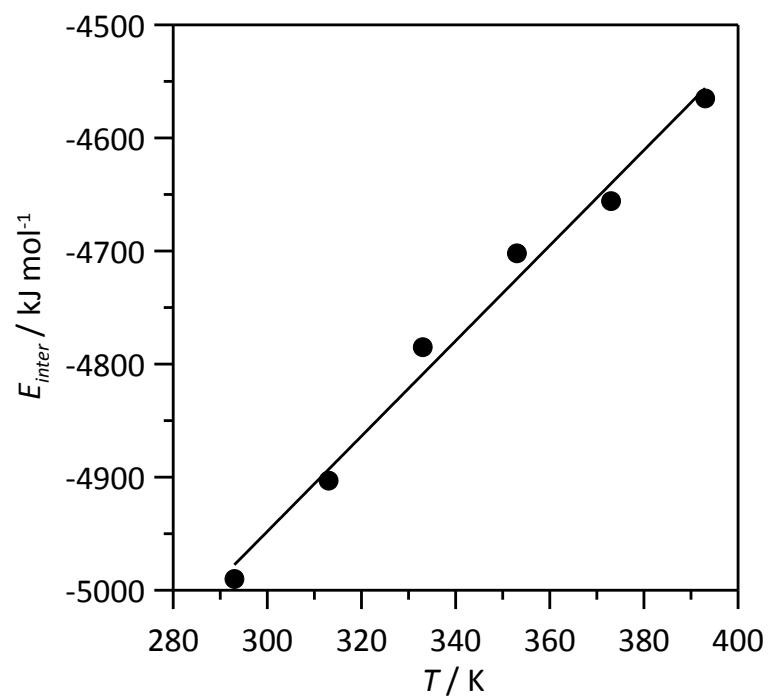
Figure 9

Figure 10

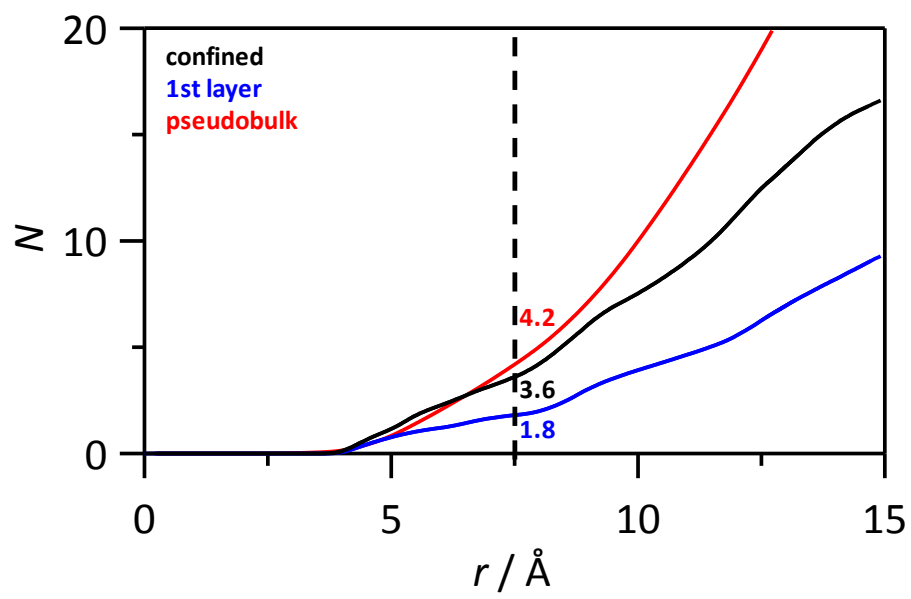**Figure 11**
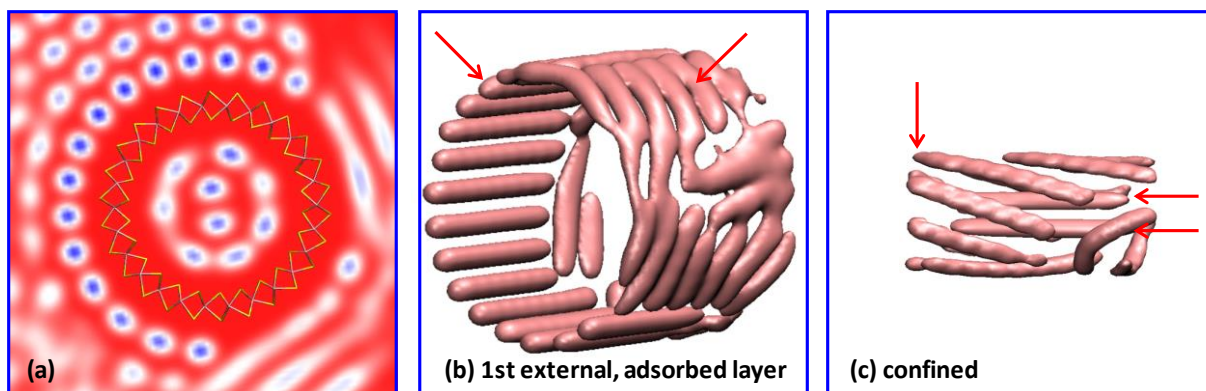
(a)

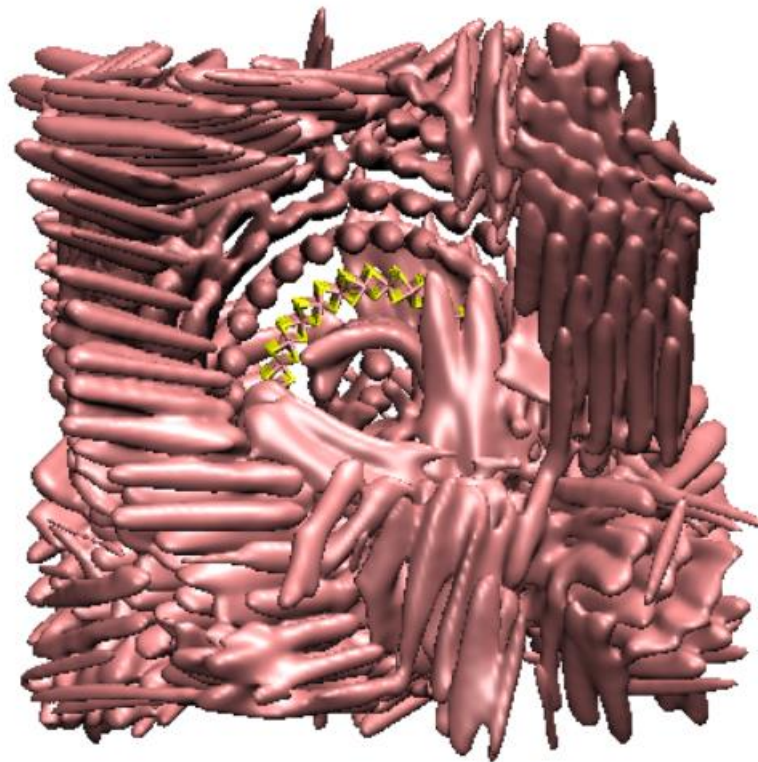(b) 1st external, adsorbed layer

(c) confined
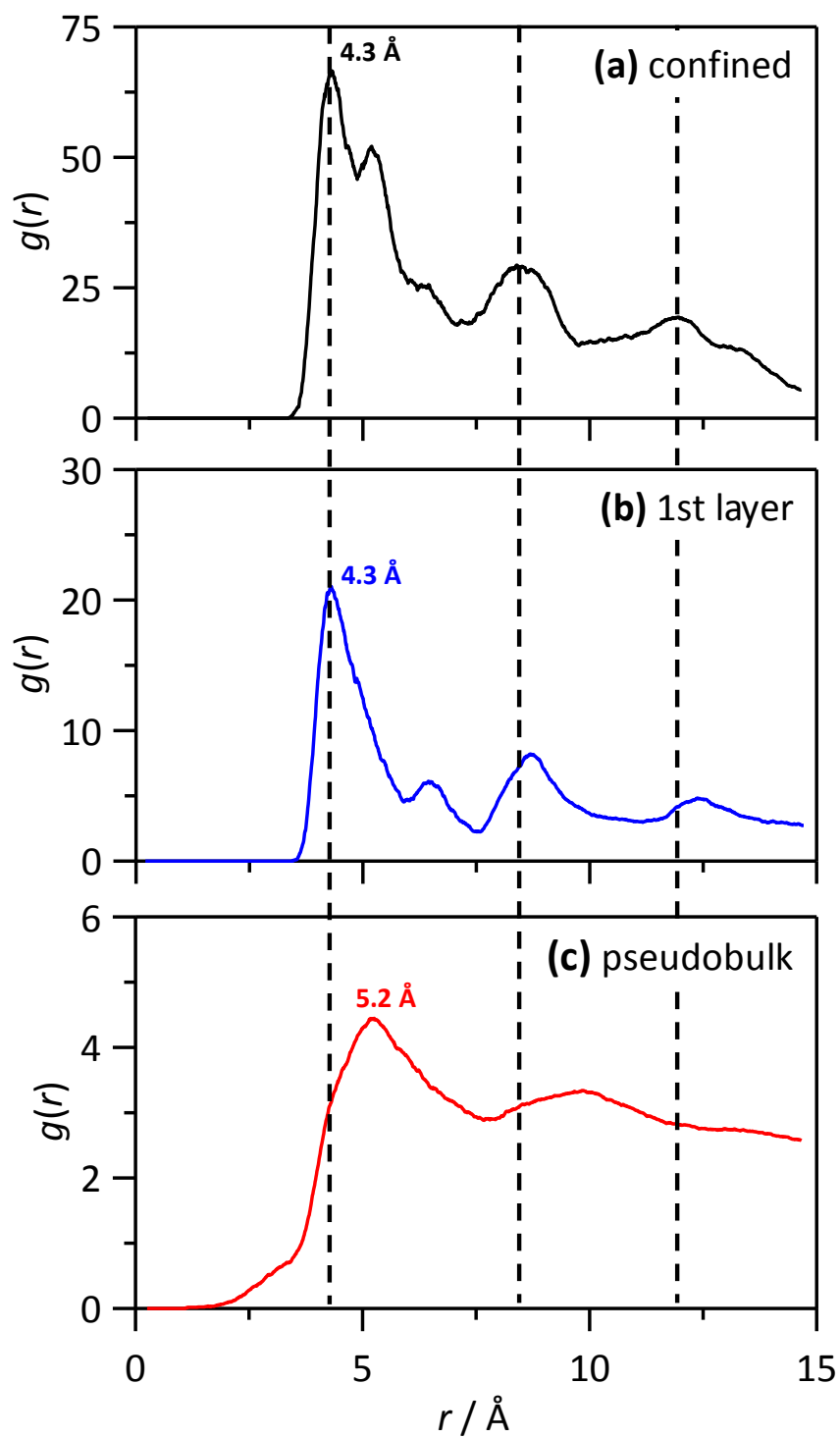
Figure 12

Figure 13

April 20, 2020

Author Statement

Manuscript title: *'Densification and tribofilm formation in hydrocarbon nanofluids induced by MoS$_2$ nanotubes'*

The individual contributions to the paper are as follows:

- Mrs. Loukia Maritsa. University of Burgos. Spain. University of Burgos. Spain. CONTRIBUTION: investigation, formal analysis, data curation, visualization.
- Prof. A. Bol. University of Burgos. Spain. CONTRIBUTION: conceptualization, methodology, resources, writing-original draft, writing-review&editing, supervision, project administration, funding acquisition.
- Prof. S. Aparicio. University of Burgos. Spain. CONTRIBUTION: conceptualization, methodology, resources, writing-original draft, writing-review&editing, supervision, project administration, funding acquisition.

Yours sincerely,

Prof. Dr. Santiago Aparicio

Department of Chemistry – University of Burgos

09001 Burgos - Spain

Tel.: +34 947 258 062

Fax.: +34 947 258 831

e-mail:sapar@ubu.es

April 20, 2020

Conflicts of Interests Statement

Manuscript title: *'Densification and tribofilm formation in hydrocarbon nanofluids induced by MoS_2 nanotubes '*

The authors whose names are listed immediately below certify that they have NO affiliations with or involvement in any organization or entity with any financial interest (such as honoraria; educational grants; participation in speakers' bureaus; membership, employment, consultancies, stock ownership, or other equity interest; and expert testimony or patent-licensing arrangements), or non-financial interest (such as personal or professional relationships, affiliations, knowledge or beliefs) in the subject matter or materials discussed in this manuscript.

Author names:
- Mrs. Loukia Maritsa. University of Burgos. Spain
- Prof. A. Bol. University of Burgos. Spain
- Prof. S. Aparicio. University of Burgos. Spain

Yours sincerely,

Prof. Dr. Santiago Aparicio

Department of Chemistry – University of Burgos

09001 Burgos - Spain

Tel.: +34 947 258 062

Fax.: +34 947 258 831

e-mail:sapar@ubu.es

Highlights

- Molecular dynamics of nanofluids.
- MoS_2 nanotubes in hydrocarbons.
- Nanotubes solvation and hydrocarbon confinement.
- Intermolecular forces for hydrocarbons confined in nanocavities.
- Lubricant oils modification by MoS_2 nanotubes.

Highlights

31